Contactless and Fine-Grained Liquid Identification Utilizing Sub-6 GHz Signals

Fei Shang, Panlong Yang, *Member, IEEE*, Yubo Yan, *Member, IEEE*, and Xiang-Yang Li, *Fellow, IEEE*

***Abstract*—The existing RF-based liquid identification systems usually rely on prior knowledge, such as pre-build database or the material and width information of the vessel. Furthermore, existing methods may not work in scenarios where the height of liquid is smaller than that of antenna. In this paper, we proposes *LiqRay*$^+$, a contactless system which can identify liquids in a fine-grained level without prior knowledge. To remove the effect of vessel, we build a dual-antenna model and craft a relative frequency response factor, exploring diversity of the permittivity in frequency domain. To eliminate the effect of different height, we devise the electric field distribution model at the receiving antenna, solving the unknown heights via spatio-differential model. Among eight different solvents, *LiqRay*$^+$ can identify alcohol solutions with a concentration difference of 1% with 92.9% accuracy. Even if the liquid height is about 4 cm, which is fairly lower than that of most antennas' heights, the accuracy is more than 85%.**

***Index Terms*—Contactless, fine-grained, liquid identification, wireless sensing.**

I. Introduction

FOR traditional liquid identification, expensive equipments are usually necessary [1], [2], [3], [4]. Benefitting from the development of ubiquitous sensing, there are lots of meaningful works [5], [6], [7], [8], [9] that are based on the communication devices being proposed for the past few years, which makes liquid identification system easier to be deployed. Based on RFID, WiFi or millimeter wave radar, Tagscan [8], Tagtag [10], WiMi [11] and FG-LiquID [12] propose clever methods to distinguish types of liquids. However, they are all data-driven systems, which therefore can't identify unknown liquids[1] that don't exist in the database. For identifying unknown liquids, LiquID [5] and Vi-Liquid [13] build models utilizing UWB and mechanical waves, respectively, to calculate the complex permittivity and viscosity characteristics, which are the inherent features of the liquids. Nonetheless, both of them require prior knowledge of the vessel (e.g., vessel material and width) to work. In many scenarios, it is difficult to pour the liquid into a known vessel. WiMi [11] implements liquid identification independent of vessel width on WiFi devices. But it can't distinguish concentration at a fine-grained level (For example, identify alcohol liquids with a concentration difference of 1%).

Furthermore, none of them consider the relative height between the liquid and the antenna: However, when the height of the liquid is less than that of the antenna, the strength of the received signal correlates with the height [14], [15], [16]. This phenomenon is common for signals in the microwave band. For example, the WiFi antenna is generally above than 12 cm, but the height of a 400ml coffee cup is about 8 cm and that of a 330ml of Coca-Cola is 10.67 cm [17]. Further, in many cases, we don't even know the height of the liquid. We add a comparison of these outstanding works in Table I.

In general, the aforementioned solutions are absent in the following two design properties:

- *First, contactless:* In many scenarios, the liquids require contactless measurement. However, if the system is built based on a vessel with a specific material and width, it may invade the liquids. Therefore, we need to eliminate the effects of vessel material and width for non-intrusive liquid identification.
- *Second, fine-grained:* There are many tested liquids in life with very small differences, such as Coca-Cola and Pepsi. On the other hand, in many scenarios, such as security checks, whether a liquid is classified as a dangerous product may depend on its concentration. Therefore, we need to identify liquids at a fine-grained level. For example, we can accurately identify the type of solvent and distinguish the liquids with a concentration difference of 1%.

In this paper?we propose a contactless and fine-grained liquid identification system, $LiqRay^+$, whose schematic diagram is shown in Fig. 1. The basic observation comes form that the complex permittivity varies with liquids, so wireless signals are attenuated differently in different liquids [18], [19], [20]. The *attenuation factor* of liquid can be utilized to construct features to distinguish liquids. However, there are three challenges needed to be solved first.

(1) The attenuation factor cannot be utilized as a feature because we cannot get the value of the attenuation factor under contactless requirements. In an RF link, the strength of the received signal is affected by the type of liquid, signal transmission distance in the liquid, the distance between the receiving

Manuscript received 24 October 2022; revised 5 June 2023; accepted 24 July 2023. Date of publication 1 August 2023; date of current version 4 April 2024. This work was supported in part by China National Natural Science Foundation with under Grant 62132018, in part by the Key Research Program of Frontier Sciences, CAS, under Grant QYZDY-SSW-JSC002, in part by the The University Synergy Innovation Program of Anhui Province with under Grant GXXT-2019-024, and in part by the NSFC with under Grants 62072424 and U20A20181. Recommended for acceptance by K. Wu. *(Corresponding author: Panlong Yang.)*

The authors are with the Department of School of Computer Science and Technology, CAS Key Laboratory of Wireless-Optical Communications, University of Science and Technology of China, Hefei, Anhui 230029, China (e-mail: shf_1998@outlook.com; plyang@ustc.edu.cn; yuboyan@ustc.edu.cn; xiangyangli@ustc.edu.cn).

Digital Object Identifier 10.1109/TMC.2023.3300356

[1]Liquids that are not in the self-built database.

TABLE I
COMPARISON OF MATERIAL IDENTIFICATION METHODS WITH WIRELESS SIGNALS

Method	Identify unknown liquids	Unlimited liquid height	Contactless		Fine-grained concentration detection(1%)
			No need to know the vessel material	No need to know the vessel width	
LiquID [5]	✔	✘	✘	✘	✘
Vi-liquid [13]	✔	✘	✘	✔	✘
TagScan [8]	✘	✘	✔	✘	✘
Tagtag [10]	✘	✘	✘	✔	✘
FG-LiquID [12]	✘	✘	✘	✔	✔
WiMi [11]	✘	✘	✘	✔	✘
LiqRay$^+$	✔	✔	✔	✔	✔

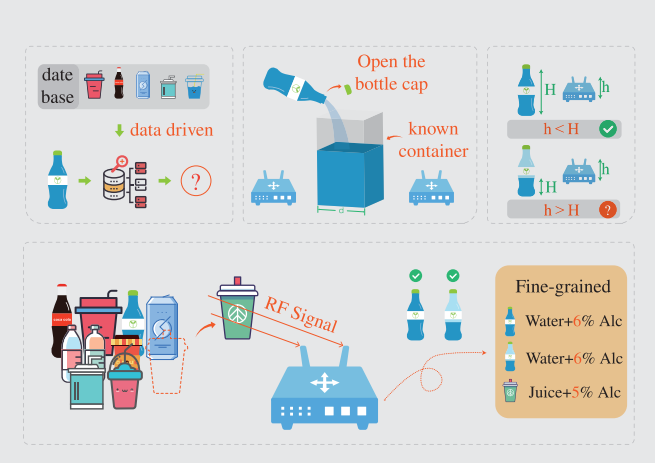

Fig. 1. Contactless and fine-grained liquid identification system, *LiqRay*$^+$.

and transmitting antennas, the vessel material, as well as the antenna gain [14], [18], [19], [21], [22]. Without relying on prior knowledge (e.g., the vessel width and material information), it is difficult to eliminate the effects of these factors and get the attenuation factor.

(2) Conventional wireless channel models may require the antenna to be lower than the liquid for effective identification. Otherwise, only a portion of the electromagnetic waves reaching the receiving antenna pass through the liquid, which makes the signal strength be related to the liquid strength. We need to remove the signal difference led by the change in height, but both the antenna's and the liquid's height are unknown.

(3) The signal attenuations are similar in liquids with similar concentrations, whereas the identification of fine-grained liquids requires the extraction of discriminative features. For example, after a 2.4 GHz electromagnetic wave transmits 5 cm in two liquids (two alcohol solutions of similar concentrations [23]) with complex permittivity of $75 + 18j$ and $80 + 19j$, the amplitude of the signal is attenuated by 0.78 times and 0.74 times, respectively. The difference is easily drowned out by noise.

Solutions: First, a dual antenna model is proposed for eliminating the effects of vessel material and antenna gain (Sections IV-A and IV-B). Founded on the fact that the attenuation factor is connected to the frequency [23], [24], [25], we extract *the relative frequency response factor* as the liquid feature, which is independent of the vessel width. Although the attenuation factors of different liquids may be similar at some frequencies [26], the change trends of the attenuation factors with frequency vary obviously from liquids [27], [28]. Taking advantage of the trend in frequency bands, the relative frequency response factor contribute to identify the liquid at a fine-grained level (Section IV-C).

Second, to eliminate the effect of liquid height, this paper models the transmitting and receiving antennas as thin straight antennas instead of a point. Combined with the distribution of the electric field in space, we extend the model to establish a functional relationship between the received signal strength and the liquid height (Section IV-E). When the transmitting antenna is displaced a small distance, the electric field below the liquid level will change. We extend the dual antenna model so that it can use this difference to extract the relative frequency response factor. In summary, we build a model-driven system to identify liquids.

Contributions: The major contributions in *LiqRay*$^+$ is threefold:

(1) We model the electric field distribution and construct a functional relationship between the received signal strength and the liquid height. Using the electric field difference when the spatial position of the transmitting antenna changes, we extend the model from 2D to 3D, which allows *LiqRay*$^+$ to identify the liquid independently of the height of the liquid and the antennas.

(2) We build a dual antenna model to eliminate the effect of the vessel material. Based on the fact that the complex permittivity of the liquid changes with frequency, we design a relative frequency response factor, the relative value of the attenuation factors at multiple frequencies, to eliminate the influence of the vessel width. Utilizing the relative frequency response factor as a feature, *LiqRay*$^+$ can identify the liquid independently of the vessel material and width.

(3) We propose *LiqRay*$^+$ to identify the concentration and types of alcohol liquid in different solvents. Even for similar solvents, such as Coca-Cola and Pepsi, *LiqRay*$^+$ can identify the alcohol concentration of 1% particle size with an accuracy rate of more than 90%. For liquids with different heights (above 4 cm), *LiqRay*$^+$ can identify liquids with a accuracy above 85.7%.

The rest of the paper is organized as follows. In Section II, we present the background of the attenuation factor, RF signal, and antenna. In Section III, we introduce the components of our system. We detail on how to remove the effects of antenna gain, that of vessel width and material, the method of identifying fine-grained liquids, and how to identify liquids without being affected by the liquid height in Section IV. In Section V, we

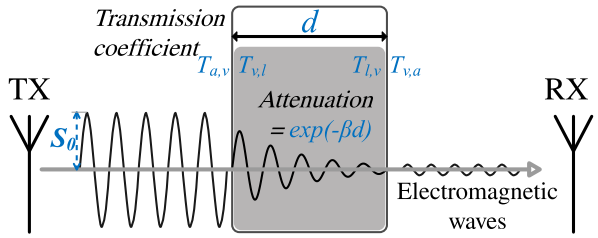

Fig. 2. Energy loss of electromagnetic waves: (1) Refraction at the interface of different media; (2)Attenuation in the medium.

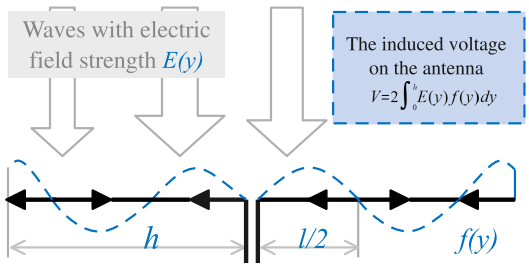

Fig. 3. Received signal strength V is the integral of the product of the electric field around the antenna and the induced current.

make extensive evaluations with several case studies to validate our system. We discuss some practical issues in Section VI and introduce the related work in Section VII. Finally, we conclude our work in Section VIII.

II. Preliminaries

A. Attenuation Factor of Liquid

Since the polarization characteristic of molecular is unique, attenuation of electromagnetic waves varies with the liquid, which provides us the opportunity to build liquid features. The attenuation can be described by the "attenuation factor", which is defined as the width of the material needed to decay the strength of the electromagnetic field to $\frac{1}{e}$ of its original value [5], [18]. For brevity, we use β to represent the reciprocal of this width, which is given by:

$$\beta = \frac{2\pi}{\lambda}\sqrt{\frac{\epsilon'\left(\sqrt{1+(\frac{\epsilon''}{\epsilon'})^2}-1\right)}{2}}, \tag{1}$$

where λ is the wavelength of electromagnetic waves in the vacuum. The real and imaginary parts of the permittivity of the liquid are denoted as ϵ' and ϵ'', respectively.

B. Signal Transmission Model

As shown in Fig. 2, the waves travel through a vessel filled with liquid to the receiving antenna. Assuming that the amplitude of the transmitted signal is S_0, that of the received signal is given by [5], [29]:

$$S_r = \alpha(D_{air})\Gamma e^{-\beta d} P S_0 \tag{2}$$

where $\alpha(D_{air})$ is the attenuation of electromagnetic waves in the air and the attenuation factor is β. The transmission distance of waves in the liquid and the gain of the receiving antenna are denoted as d and P, respectively. Besides, the transmission loss at the interface of two dielectrics is expressed as Γ, which is the product of the transmission coefficients across the four interfaces, including two air-vessel interfaces ($T_{a,v},\ T_{v,a}$) and two vessel-liquid interfaces ($T_{v,l},\ T_{l,v}$). When electromagnetic waves are transmitted to the interface of two media (e.g., air and vessel wall), they will be refracted and reflected, and part of this energy can be transmitted to the new medium [30], [31], [32]. The fraction of penetrated energy is given by the transmission coefficient T, which is given by [33]:

$$T = \sqrt{\frac{1}{2}\epsilon'\left(1+\sqrt{1+(\epsilon''/\epsilon')^2}\right)} \tag{3}$$

where ϵ' and ϵ'' are the real and imaginary part of the complex permeability, respectively.

C. The Relationship Between Signal Strength and Electric Field Distribution

Since the attenuation of electromagnetic waves are different in the air and liquid [34], [35], the distribution of electric field around the receiving antenna is related to the liquid height. Therefore, the induced voltage on receiving antenna is affected by the height. For identifying liquids independent of the height, we explore the relationship between the electric field distribution and the induced voltage.

As shown in Fig. 3, a beam of electromagnetic waves, whose electric field strength is $E(y)$, incidents an antenna along the negative direction of the x-axis (perpendicular to the antenna). The direction of field is the positive direction of y-axis (parallel to the antenna). For the antenna which is fed symmetrically by a balanced two-wire transmission line, the total induced voltage V is given by [14], [36], [37]:

$$V = 2\int_0^h E(y)f(y)dy \tag{4}$$

where $2h$ is length of the antennas that is symmetrical about the midpoint, and the current distribution at y is $f(y)$, which is shown in Fig. 3.

III. Overview

LiqRay $^+$ consists of two major components: data preprocessing, and identify the liquid. We utilize a transmitting antenna and two receiving antennas to construct our system. The system overview is shown in Fig. 4.

Data Preprocessing: We process the data collected from the two receiving antennas separately. The data is first filtered and smoothed to suppress noise. Then the Tx movement detection is performed to determine the time when the transmitting antenna starts to rise. Subsequently, a segment of the data is intercepted to identify the liquid.

Identify the Liquid: We construct an electric field distribution model and control the transmitting antenna to rise a certain

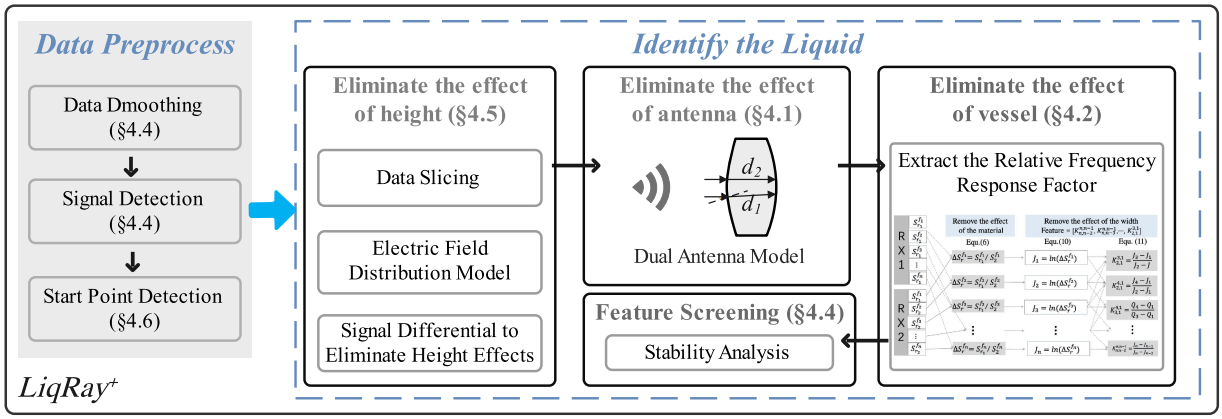

Fig. 4. System Overview. Having preprocessed the data, we judge whether the liquid is higher than the antenna. If the height of liquid is less than that of antenna, we first remove the effect of height. Then, we construct the relative frequency response factor that is independent of the width and material of vessel to identify the liquids.

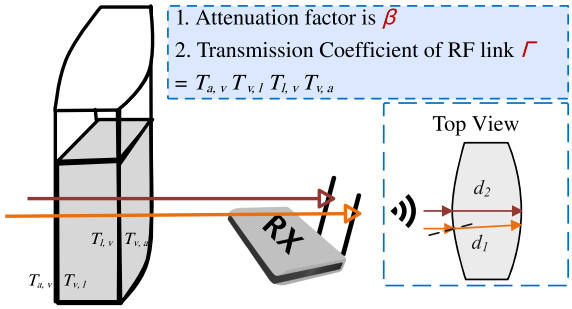

Fig. 5. Dual antenna model. Signals are refracted and attenuated during transmission.

distance by a motor. We use the difference of the electric field caused by the displacement of the transmitting antenna to remove the effect of the liquid height (Section IV-E). The intensity of received signal is affected by the material and width of the vessel, as well as the attenuation factor. We extract the attenuation factor of the liquid to construct feature to achieve the purpose of knowing the liquid in a fine-grained level. Since the vessel material has similar effects on the signal strength of the two RF links, we combine the two antenna signals to remove the influence of the vessel material (Section IV-B). Moreover, we take advantage of the different attenuation of signals of different frequencies in the liquid to remove the influence of the width of the vessel (Section IV-B). Finally we introduce how the system achieves fine-grained levels in Section IV-C.

IV. System Design

A. Eliminate the Effect of Antenna

As shown in Fig. 5, we build a dual-antenna model to eliminate the effect of antenna gain. The basic idea is that the effects are similar for the two RF links.

This paper denote that the signal transmission distance in the liquid of two RF link are d_1 and d_2, respectively, and that in the air are D_1 and D_2, respectively. Similar to (2), the strength of received signals are given by:

$$S_{r1} = \alpha(D_1)\Gamma_1 e^{-\beta d_1} P S_0$$
$$S_{r2} = \alpha(D_2)\Gamma_2 e^{-\beta d_2} P S_0 \quad (5)$$

where P is the receiving antenna gain and β is the attenuation factor. We utilize $\alpha(.)$ to denote the decay in the air and use Γ to denote the transport coefficient at medium interface.

Since the distance between two receiving antennas is much less than that between the receiving antenna and the transmitting antenna, we believe that $D_1 \approx D_2$. As the type of two antennas are same, we can get

$$\Delta S_r = \frac{S_{r1}}{S_{r2}} = \Delta\Gamma e^{-\beta\Delta d} \quad (6)$$

where $\Delta\Gamma = \Gamma_1/\Gamma_2$, $\Delta d = d_1 - d_2$, and ΔS_r is independent of the antenna gain P. In this equation, we use $\Delta\Gamma$ to represent the ratio of refraction's influence on the two RF amplitudes. LiqRay [38] ignores the influence of the incident angle of the signal on the refraction when designing the liquid characteristics, which is feasible when the vessel is perpendicular to the incident wave, but the liquid identification will be affected after the vessel is tilted to a certain extent. To address this shortcoming, we try to reconstruct the relative frequency response factor and rely on the opportunity presented by the frequency change to eliminate the effect of the vessel material without relying on this assumption.

B. Eliminate the Effect of Vessel

For constructing a feature which is only related the type of liquid, we would better calculate the value of attenuation factor. However, as shown in (6), the vessel influence is reflected in two aspects ($\Delta\Gamma$ and Δd), which hinder the extraction of attenuation factor β. Utilizing the characteristic of complex permittivity as a function of frequency, we construct the relative frequency response factor that is independent of the vessel.

It is Difficult to Eliminate the Effect of Vessel: On the one hand, the transport coefficient varies $\Delta\Gamma$ with vessel material, while it is inconvenient to pre-obtained material information. On the other hand, the signal transmission distance Δd and

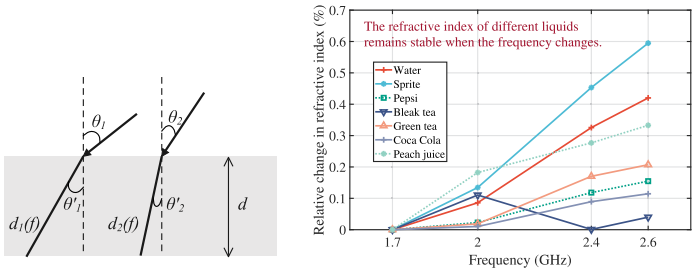

Fig. 6. Effect of frequency on d can be ignored. (a) The transmission distances. (b) The refractive index remains stable.

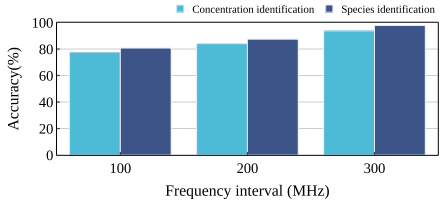

Fig. 7. Using four frequency points, the accuracy of liquid identification when the frequency interval is different.

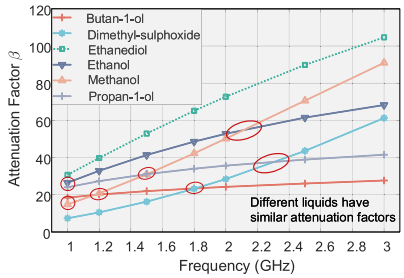

Fig. 8. Different liquids may have similar attenuation factors.

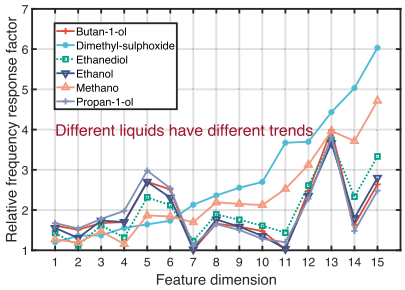

Fig. 9. Different liquids have unique relative frequency response factors.

the attenuation factor β are coupled together, which make it is difficult to be solved by adding RF links.

Fortunately, the Frequency Domain Presents us With an Opportunity: The key idea comes from a fundamental observation: the refractive index of a medium varies little with frequency and the attenuation factor varies greatly with frequency. Therefore, we approximate the refractive index as not changing with frequency. The impact of the container on the signal amplitude mainly comes from two aspects: the refraction of the medium and the transmission distance of the signal in the liquid, both of which are related to the refractive index. As a result, the effect of the container on the signal amplitude is almost invariant with frequency. This gives us the opportunity to use ratios of different frequency signals to remove its effect.

In particular, when the signal frequency is changed, the effect of vessel keeps stable while the attenuation factor β of different liquids has different trends [18], [39]. Thus, it is possible to eliminate the "static" variables ($\Delta\Gamma$ and Δd) with signals of multiple frequencies. As shown in (1) and (3), the transport coefficient Γ is depended on the complex permittivity. Furthermore, the transmission distance d is related to the vessel width and the refraction angle, which is related to the transmission coefficient according to the Fresnel's law [40].

Since the change of transmission coefficient is small, we believe that $\Delta\Gamma$ and Δd is the constant. We notice that the thickness of the container wall is relatively small (for example, the thickness of the container we chose is about 3 mm), and the refractive index of common non-metallic container materials is relatively small (for example, the refractive index of glass is about 1.5, while the refractive index of water is close to 9), so we ignore its influence on the signal propagation path $d(f)$ and only consider its influence on the signal amplitude. As shown in Fig. 6(a), the difference in transmission path is given by

$$\Delta d(f) = d_1(f) - d_2(f) = \frac{d}{cos\theta'_1} - \frac{d}{cos\theta'_2}, \tag{7}$$

where d is the width of the vessel, f is the frequency of the signals, and θ'_1 and θ'_2 are the angles of refraction of the RF signals. According to the Fresnel equation [41], the relationship between the angle of incidence, θ, and the angle of refraction, θ', is

$$\frac{sin\theta}{sin\theta'} = n_r(f), \tag{8}$$

where n_r is the relative refractive index of the liquid and air, which is related to the frequency. As a result,

$$\Delta d(f) = \frac{d}{\sqrt{1 - \left[\frac{sin\theta_1}{n_r(f)}\right]^2}} - \frac{d}{\sqrt{1 - \left[\frac{sin\theta_2}{n_r(f)}\right]^2}}, \tag{9}$$

Fig. 6(b) shows the transmission coefficient's relative variation with frequency of seven common liquids, which is calculated by (3). The change in the value of the transmission coefficient at 2.6 GHz is less than 0.6% compared to that at 1.7 GHz, i.e., $n_r(f) \geq 0.994 n_r(1.7\,\text{GHz})$ for $1.7\,\text{GHz} \geq f \geq 2.6\,\text{GHz}$. Note that the refractive index of the liquid to be measured is usually greater than 8, and the change of nr with frequency will hardly cause the change of $\Delta d(f)$. Therefore, we treat $\Delta d(f)$ as a frequency-independent quantity for subsequent calculations. On the contrary, due to the different molecular polarization characteristics, the trend of the attenuation factor with frequency varies with the liquid type [23], [33], [42].

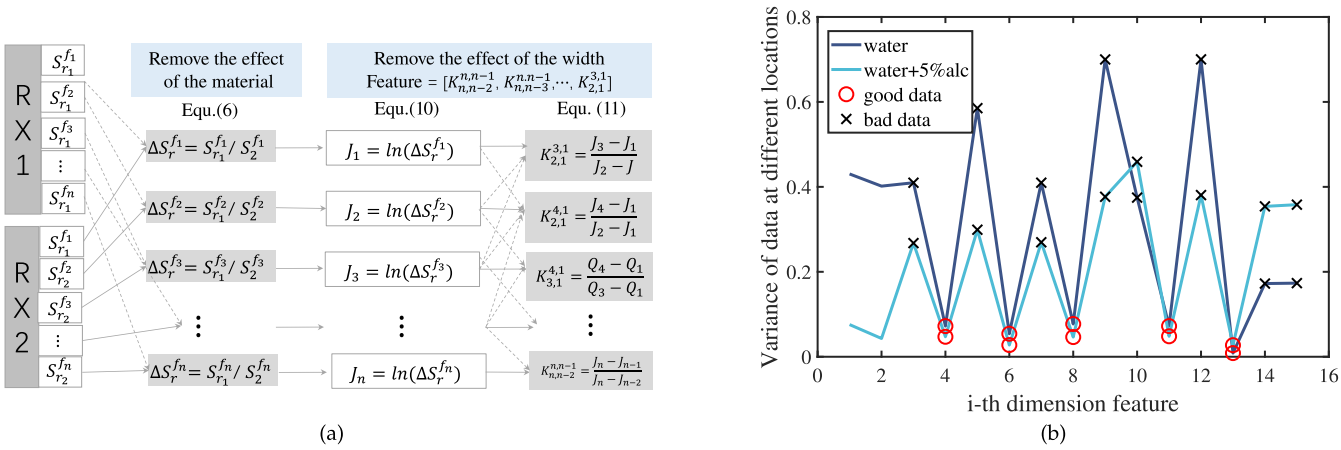

Fig. 10. Data processing flow and data characteristics. (a) Using the signals of different frequencies to remove the influence of vessel material and width. (b) Collecting data at different locations has large differences in the stability of features in different dimensions.

Extract Vessel-Independent Relative Frequency Response Factor: In the case that neither the vessel nor the liquid is changed, we collect the signal intensity of electromagnetic waves of different frequencies and form a set $\Delta S_R = [\Delta S_r^{f_1}, \Delta S_r^{f_2}, \ldots, \Delta S_r^{f_n}]$, where f_i is the i-th frequency. When $i \neq j$, we can get:

$$J_{i,j} = \frac{\Delta S_r^{f_i}}{\Delta S_r^{f_j}} = e^{(\beta(f_j) - \beta(f_i))\Delta d} \tag{10}$$

For $(p, q) \neq (u, v)$,

$$K_{u,v}^{p,q} = \frac{ln(J_{p,q})}{ln(J_{u,v})} = \frac{\beta(f_p) - \beta(f_q)}{\beta(f_u) - \beta(f_v)} \tag{11}$$

When p, q, u, v change from N to 1, we can get the **relative frequency response factor** $F = [K^{N,N-1}_{N,N-2}, \ldots, K^{3,1}_{2,1}]$, whose dimensions are $\binom{N}{2}$, where $\binom{n}{k} = \frac{n!}{(n-k)!k!}$. The whole process is shown in Fig. 10(a).

C. Fine-Grained Identification of Liquids

Based on the attenuation factor, we take the relative frequency response as the feature of the liquid and use a small amount of frequency band resources to complete the recognizing of the fine-grained liquid.

The relative frequency response factors is a unique feature which helps us identify the liquid in a fine-grained level. The reason why similar liquids are indistinguishable is that they have so similar attenuation factors that the attenuation of signals are almost the same. To make matters worse, two liquids that look dissimilar may also have similar attenuation factors. Fig. 8 shows the attenuation factors for six different liquids (calculated according to complex ermittivities [26] of different frequencies using (1)). In the red circles, the attenuation factors are similar. However, the relative frequency response factor exhibits more unique feature. Relative frequency response factors of the six liquids are shown in Fig. 9 where different liquids have different "frequency response" curve. We believe the reason is that the relative frequency response factor reflects the more essential characteristics of the liquid. Due to the different polarization characteristics of different molecules, the changing trend of the attenuation factor with frequency is different for different liquids [43], [44], which makes the relative frequency response factors can be used to identify liquids at a fine-grained level.

D. Details of Data Processing

Select the Frequencies of the Carriers: With eight common beverages as solvents, including water, Pepsi, Sprite, Cola, Master Kong Iced Black Tea, Master Kong Green Tea, Huiyuan Orange Juice, and Huiyuan Peach Juice, we formulate alcohol solutions with concentrations varying from 1% to 20%. A 3D printed resin vessel whose size is 8 cm×30 cm×30 cm are utilized for holding that liquids. We first evaluated the frequency interval. The minimum frequency of each experiment is 1.7 GHz. The set frequency intervals are 100 MHz, 200 MHz, and 300 MHz, respectively. The results are shown in Fig. 7. We find that larger frequency intervals lead to higher accuracy. We believe this is due to the fact that the attenuation factor varies more significantly with frequency than the refractive index. Next we evaluated the effect of the number of frequencies.

The signal frequencies are 1.7 GHz, 2.0 GHz, 2.4 GHz, 2.6 GHz and 5.0 GHz. Then we use the k-nearest neighbor algorithm (k = 1) to identify the liquid. For the single frequency, we use the amplitude ratio of two receiving antennas as the feature (6), and for multiple frequencies, we extract the relative frequency response factor as the feature. As shown in Table II, the accuracy is significantly improved is we use the relative frequency response factor as liquid feature. Besides, we find that 4 frequency points can already identify liquids in a fine-grained level, and the antenna can only work in a specific frequency band (for example, the frequency band width of the antenna we choose to work continuously is about 1 GHz). As a result, we select 1.7 GHz, 2.0 GHz, 2.4 GHz and 2.6 GHz to use.

Data Smoothing and Signal Extraction: After the liquid is presented in the RF link, the amplitude of the signal is significantly attenuated. We utilize a sliding window to continuously

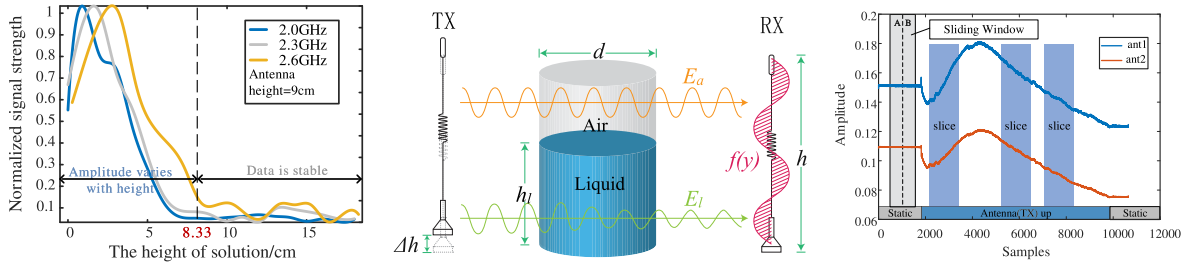

Fig. 11. Height-corrected Model. (a) When the liquid height is less than the antenna height, the liquid height will affect the signal strength. (b) When the depth of the liquid is less than the height of the antenna, the signal received by the receiving antenna consists of two parts: (1) E_l that reaches the receiving antenna through the liquid; (2) E_a that reaches the receiving antenna through the air. (c) The data collected by the two receiving antennas when the transmitting antenna is slowly raised. We utilize sliding time windows for start point detection and random slices for liquid feature extraction.

TABLE II
ACCURACY OF IDENTIFICATION WITH DIFFERENT SIGNALS

Frequency (GHz)	Accuracy rate of concentration identification	Accuracy rate of species identification
1.7	65.53%	73.33%
2.0	73.74%	77.93%
2.4	55.38%	63.64%
2.6	70.49%	74.07%
5.0	74.66%	77.12%
1.7,2.0,2.4	85.44%	86.38%
1.7,2.6,5.0	89.33%	91.02%
1.7,2.0, 2.4, 2.6	92.9%	96.78%
1.7,2.0, 2.4, 2.6, 5.0	96.66%	98.04%

detect whether the liquid is present in RF link. The variance of the amplitude value in sliding window reflects the degree of amplitude fluctuation. When the amplitude decreases and the variance is large, we consider a liquid to be placed in RF link; when the amplitude is increasing and the variance is large, this paper considers a liquids to be taken out.

Feature Screening: We utilize four frequencies including 1.7 GHz, 2.0 GHz, 2.4 GHz, and 2.6 GHz. The water and 5% alcohol are used as the test liquid to collect data 50 times independently. The variance of each dimension feature is calculated. We find that feature stability varies widely across dimensions. The result is shown in the Fig. 10(b). We use red circles to mark data points with good stability, and use black crosses to indicate data points with poor stability. We believe the reasons are given by: (1) Interference from other signals, such as WiFi signals in the 2.4 G band; (2) $ln(.)$ operations and division operations amplify signal errors. Therefore, we use variance to filter the dimensions with stable and use them as the final liquid feature.

E. Eliminate the Effect of Height

Although we have designed a vessel-independent feature, it is difficult to identify liquid with the signals around 2.4 GHz. The reason is that the signal strength is related to the relative height of antenna and liquid [45]. Unfortunately, there are many antennas that is used for receiving the signals with a frequency about 2.4 GHz are higher than 15 cm, while the beverages that are lower than 15 cm are common.

For eliminating the height effect, we construct a electric field distribution model around the receiving antenna and establish a functional relationship between the signal strength and liquid height. Utilizing the opportunity presented by the movement of the transmitting antenna in space, the effect of height is eliminated.

Liquid Height Affects Signal Strength: With the 9 cm antenna, we add water with different heights to a resin vessel (length, width, and height are 60 cm × 60 cm × 40 cm). We test the signals of 2.0 GHz, 2.3 GHz and 2.6 GHz respectively. As shown in Fig. 11(a), the signal strength varies with the height when the liquid is lower than antenna. To weaken this problem by a model-driven way, we try to analyze the field around the receiving antenna.

Electric Field Distribution Model: As shown in Fig. 11(b), the liquid height is h_l, and the height of receiving antenna is h. When h is bigger than h_l, the signals near the receiving antenna can be divided into two parts: (1) transmitted from the liquid, the field strength is E_l; (2) transmitted from the air is E_a. Since the vessel is in the far-field region of the transmitting antenna, we assume that the incident waves is the plane electromagnetic wave [14]. As a result, with a frequency of f, the electric field $\mathbf{E_a}$ and $\mathbf{E_l}$ are given by:

$$\begin{aligned} \mathbf{E_a} &= \Gamma_a \alpha_a \mathbf{E_0} \\ \mathbf{E_l} &= \Gamma_l \alpha_l \exp(-\beta d)\mathbf{E_0} \end{aligned} \tag{12}$$

where d is the transmission distance in liquid, and β is the attenuation factor. The transmission losses are denoted as Γ_a and Γ_l. The attenuation in the air is represented as α. With the unit vector in the vertical direction $\mathbf{e_y}$, the electric field are given by $\mathbf{E_a} = E_a\mathbf{e_y}$ and $\mathbf{E_l} = E_l\mathbf{e_y}$, respectively.

For brevity's sake, we define $\gamma = \frac{T_l \alpha_l}{T_a \alpha_a}$. And the E_l can be expressed as

$$E_l = \gamma \exp(-\beta d) E_a \tag{13}$$

According to (4), the signal strength S_r^0 on the antenna is derived by:

$$S_r^0 = \int_0^{h_l} E_l f(y) dy + \int_{h_l}^{h} E_a f(y) dy$$

$$= \gamma \exp(-\beta d) E_a \int_0^{h_l} f(y)dy + E_a \int_{h_l}^{h} f(y)dy \quad (14)$$

where $f(y)$ is the distribution of induced current on the antenna, which is related to the type of antenna and the wavelength of the signal.

Signal Differential to Eliminate Height Effects: We collect signals at different height. Every Δh collects the signal strength on the receiving antenna to obtain a sequence $A = [a_0, a_1, \ldots, a_{n-1}]$, where

$$a_j = S_r^j = \int_{j\Delta h}^{h_l} E_l f(y)dy + \int_{h_l}^{h} E_a f(y)dy$$

$$= \gamma \exp(-\beta d) E_a \int_{j\Delta h}^{h_l} f(y)dy + E_a \int_{h_l}^{h} f(y)dy \quad (15)$$

As a result,

$$a_{j+1} - a_j = \gamma \exp(-\beta d) E_a \int_{j\Delta h}^{(j+1)\Delta h} f(y)dy$$

$$= \gamma \exp(-\beta d) E_a f(j\Delta h)\Delta h \quad (16)$$

Two receiving antennas are utilized in our system, and we compute $\Delta a = a_{j+1} - a_j$ separately on both antennas:

$$\Delta a_{rx1} = \gamma \exp(-\beta d_1) E_a f(j\Delta h)\Delta h$$
$$\Delta a_{rx2} = \gamma \exp(-\beta d_2) E_a f(j\Delta h)\Delta h \quad (17)$$

We calculate their ratio to get:

$$\frac{\Delta a_{rx1}}{\Delta a_{rx2}} = exp(-\beta \Delta d) \quad (18)$$

where $\Delta d = d_1 - d_2$.

Eq. (18) is independent of the height. Since that (18) and (6) have the exact same form. we utilize the method in Section IV-B for subsequent processing to obtain the liquid feature.

F. Implementation Details

Tx Movement Detection: The signals we collected consist of a three-stage process: (1) the transmitting antenna is stationary; (2) the transmitting antenna is moved upward; (3) the transmitting antenna is stationary. For identifying the liquid, we slice the signals when the transmitting antenna is raised. Similar to WiFi's packet detection, we utilize the double sliding windows packet detection algorithm to detect the start point of the signal, which is shown in Fig. 11(c). We set up two sliding windows A and B, whose width are both L. Then we calculate the ratio of the energies of the signals in the two windows [46]:

$$ra_i = \frac{\sum_{m=0}^{L-1} r_{i-m} r_{i-m}^*}{\sum_{l=1}^{L} r_{i+l} r_{i+l}^*}, \quad (19)$$

where r is the amplitude of the signal, and r^* is the conjugate of r, and i is the right edge of window A. With the window sliding from left to right and a signal series of length N, we get the set $Ra = [ra_{L-1}, \ldots, ra_{N-L-1}]$. Furthermore, we calculate the difference of Ra, $Dra = diff(Ra)$. Since the signal strength in the stationary phase is relatively stable, when both windows contain only the signal in the static, the value of Dra is small. However, when one window only contains the signal in the static and the other window contains the signal in the antenna rising, the value of Dra begins to change rapidly. If the value of Dra at i is greater than 50 times the value of Dra at rest, we believe the antenna to start to rise.

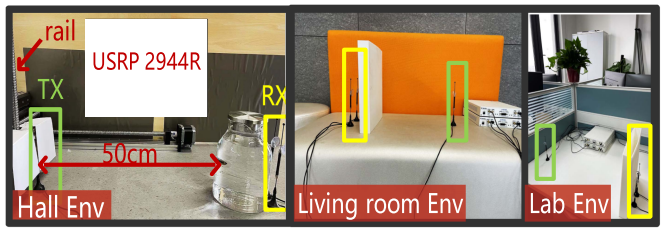

Fig. 12. Experimental deployment.

Clustering and Selecting Stable Slices: As shown in (16), we only need the data of two adjacent positions to obtain the liquid feature. Nevertheless, since random noise and other factors, Δa may not be able to perform subsequent processing. For each frequency, we randomly calculate a slice (width is 1000 samples). For those slices, we fit a 5th order polynomial to the data, which are utilized to calculate the relative attenuation factor. We cluster the attenuation factors for each dimension (choose 0.2 for the inter-class distance) [47]. Then check if the number of samples in the largest class exceeds 50% of the total. If the number of dimensions satisfying the condition is less than 3, we re-slice the signal. Since factors such as sampling error, we make the TX rise at least 2 cm to ensure that we have enough data to select data.

V. Evaluation

A. Experimental Setup

Hardware Setup: The NI company's N2944R USRP devices are used as the transmitter and receiver, which are shown in Fig. 12. The antennas is able to send and receive wireless signals with the frequency range of 698-960MHz, 1700-2700MHz, and 4900-5850MHz. We use a computer with Intel i7-10700 CPU and 16 G memory to process the RF data.

Experimental environments: As shown in Fig. 12, the USRP devices are placed 3m away from the antennas, and we place vessel in the direct path. For collecting data, we continue to send a sine signal at frequencies of 1.7 GHz, 2 GHz, 2.4 GHz, and 2.6 GHz,respectively.

Data Collection: For each liquids, we perform 50 independent data collections. The temperature of all liquids is at room temperature. For the effect of height and container on liquid identification, we adopt a similar verification method to the effect of the test packets. For example, if we test the accuracy of the system to identify the liquid when the liquid height is 4 cm, we use the data collected when the liquid height is 4 cm as the test data, and use the data collected when the liquid height is other values to construct the KNN classifier. For other tests, we use five-fold cross-validation to test the accuracy of liquid recognition. We have revised the description of the relevant part

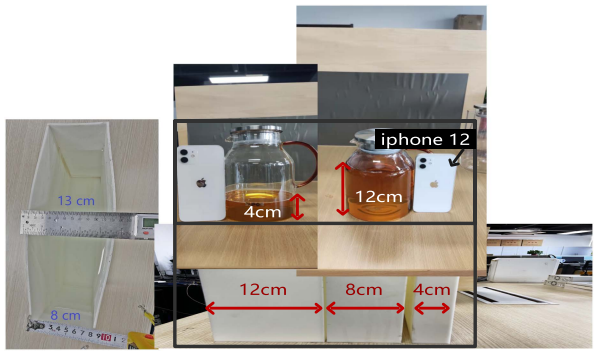

Fig. 13. Experimental vessel. (a) Top view of the resin container. (b) Resin containers of different widths and liquids to be tested at different heights.

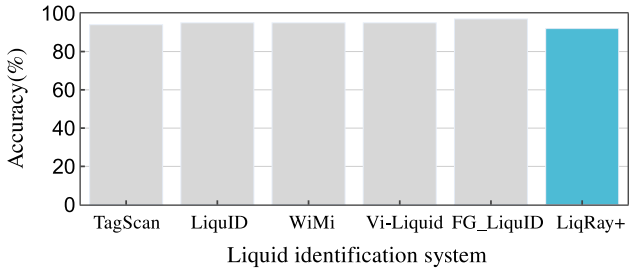

Fig. 14. Accuracy of related work.

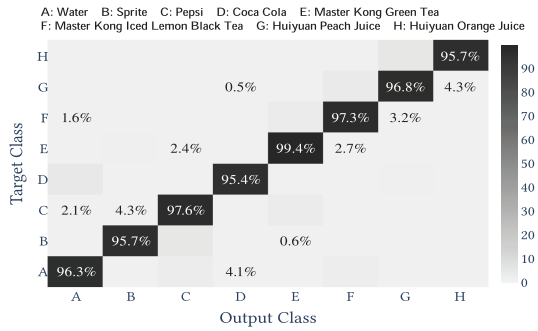

Fig. 15. Identification performance for 8 liquids.

of the paper to avoid it confusing the reader. In this paper, we define accuracy as the ratio of the number of correctly classified samples to the total number of samples.

B. Micro Benchmark

Experimental Settings: Eight common beverages are used for solvents, in which we dissolve alcohol in concentrations ranging from 0% to 20%, and then identify them. We utilize a 3D printed resin vessel (8 cm × 30 cm × 30 cm, which is shown in Fig. 13(a)), to hold the liquid.

Fine-Grained Solutions Identification: We test eight different solvents, including Coca-Cola, Master Kong Green Tea (a tea beverage), Pepsi, Master Kong Ice Black Tea (a tea beverage), Orange juice, Peach juice, water, and Sprite. The alcohol concentration changes from 0 to 20% in 1% steps. The data are collected

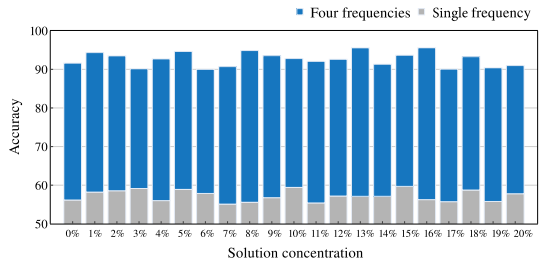

Fig. 16. Identification performance of alcohol solutions with different solvents.

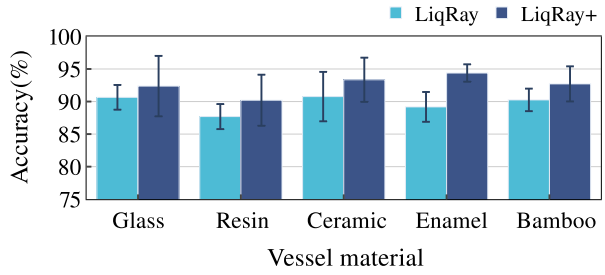

Fig. 17. Impact of vessel material.

100 times independently for each concentration. Utilizing the relative attenuation factor (with 4 frequencies) as feature, we adopt a simple K-Nearest Neighbors algorithm (K=1) to differentiate those liquids. The result are shown in Fig. 16. *LiqRay*$^+$ achieves an average accuracy of 92.9%. Fig. 15 demonstrates *LiqRay*$^+$'s ability to identify solvents with an average accuracy of 96.78%.

Fig. 14 shows how *LiqRay*$^+$ compares with some excellent related work. We find that these works are similar in terms of liquid identification. However, compared with related work, *LiqRay*$^+$ only needs to collect data at a few frequency points, which does not occupy high bandwidth resources. We believe that the reason is that the relative frequency response factor is constructed as a feature by using the characteristic that the complex permittivity of liquid varies with frequency, which eliminates the adverse effects of vessel on liquid identification.

Impact of Vessel Material: We pour the liquids into five different material vessels (both have a radius of 5 cm), including ceramic, glass, resin, enamel, and bamboo. The liquids are with different concentrations from 0% to 10% at a step size of 1%. The solvents are Coca-Cola, Sprite, Pepsi, and water. Fig. 17 shows the results. The average accuracy of concentration identification is 92.6% . Vessel of different materials have similar accuracy rates.

The results shows that, despite the change in the material of the vessels, *LiqRay*$^+$ still accurately identified liquids. We believe the reason is that we design the relative frequency response factor as a feature, which suppresses the influence of the material through the ratio method. However, unfortunately, limited by the characteristics of RF signal, it will produce significant attenuation after passing through the metal vessel, which makes it difficult for the system to detect the liquid contained in the metal vessel.

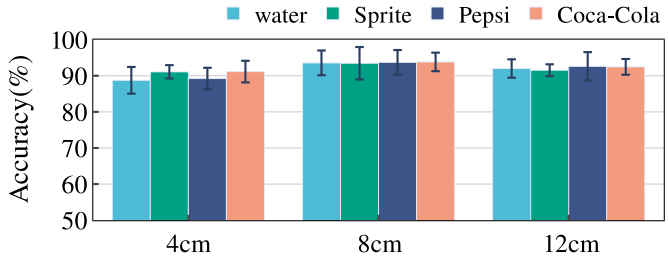

Fig. 18. Impact of vessel width.

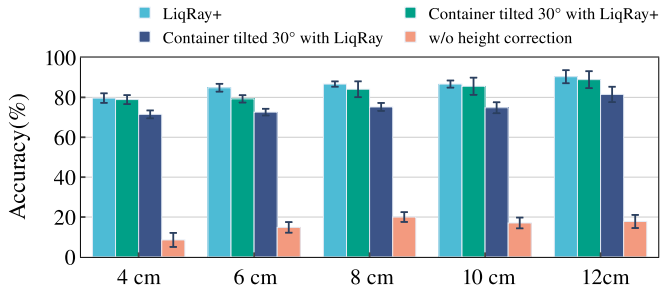

Fig. 19. Impact of different heights.

Compared with the features used by LiqRay [38], *LiqRay*$^+$ improves the accuracy by about 5% after redesigning the features. We believe the reason is that the features we designed are more insensitive to differences caused by materials.

Impact of Vessel Width: The liquids are poured into vessels with three different width (including 4 cm, 8 cm and 12 cm), which are shown in Fig. 13(b). The concentration of liquids is from 0% to 10% at a step size of 1%, 45%, 46% and 78% and different solvents with Coca-Cola, Sprite, Pepsi and water. As shown in Fig. 18, for different width vessel, *LiqRay*$^+$ can identify the liquid with more than 90% accuracy. However, as the width of the vessel increases, the attenuation of the signal increases, which reduces the accuracy.

Thanks to the relative frequency response factor which eliminates the influence of the vessel width, *LiqRay*$^+$ can still accurately identify the liquid when the vessel width is changed. When the width of the vessel is greater, the difference between the two RF links is greater, which helps to differentiate liquids. However, wider distances result in more severe attenuation, which results in a worse signal-to-noise ratio. As a result, it may interfere with liquid identification. We plan to investigate in future work how to balance the two aspects.

Impact of Liquid Height: Six heights including 3 cm, 4 cm, 6 cm, 8 cm, 10 cm and 12 cm are tested. The data are collected on eight different beverages for each height. For each beverage, we collect 50 times independently. With a motor controlling the transmit antenna up or down. we collect data on when the vessel is upright and when the vessel is tilted 30 degrees. Having obtained the relative attenuation factor (with 4 frequencies) as features, we can adopt a simple K-Nearest Neighbors algorithm to identify those liquids. For each test, one height of data are used as the test set and others are used to construct the KNN classifier. Fig. 19 shows the results. We test the results of directly extracting features, but the accuracy is only 15.7%. However, befitting from the method in Section IV-E, *LiqRay*$^+$ can identify the liquids with a accuracy of 85.7%.

We believe the reason is that the poor stability of the data when the motor starts to raise. When the liquid height is small, the duration of the signal containing the liquid information is short. Therefore, it isn't conducive to the screening of data. Furthermore, we test the identification ability of directly extracting features for identification without high calibration. And the accuracy is poor, which is only 15.7%. The reason may be that when the height of the liquid is lower than that of the antenna, a part of the EM waves reach the receiving antenna

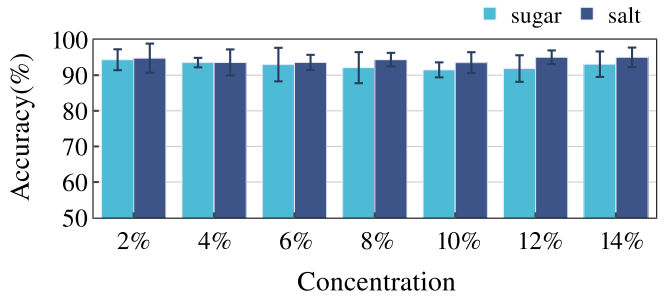

Fig. 20. Accuracy in identifying NaCl and sucrose.

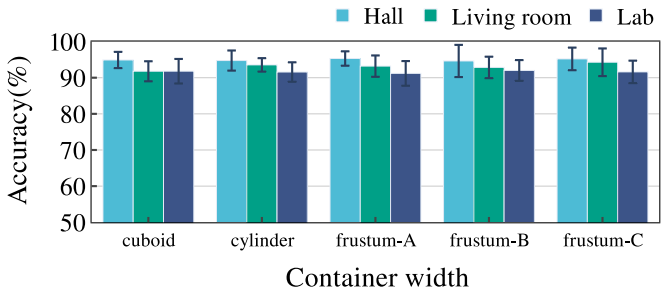

Fig. 21. Accuracy of using different shapes vessels to hold liquids in different environments.

without passing through the liquid. since the proportion of this part of the EM waves are affected by the liquid height, the accuracy of identifying utilizing the unprocessed signal is poor. And *LiqRay*$^+$ can extract the signal passing through the liquid transmission part. As a result, it can identify the liquid independent of height.

When the vessel is tilted to a certain extent, *LiqRay*$^+$'s accuracy of identifying liquids changes less. However, the accuracy of LiqRay [38] has dropped significantly. We believe that this is because LiqRay [38] ignores the influence of the incident angle of the signal on the refraction when designing the liquid features. This is feasible when the vessel is perpendicular to the incident wave, but when the vessel is titled, it will affect the liquid identification. Whereas *LiqRay*$^+$ does not rely on this assumption when building traits and therefore has better performance.

Impact of the Liquid Temperature: We use drinking water as the solvent and alcohol as the solute. The concentration of alcohol varies from 0 to 20% in steps of 1%. We collect data

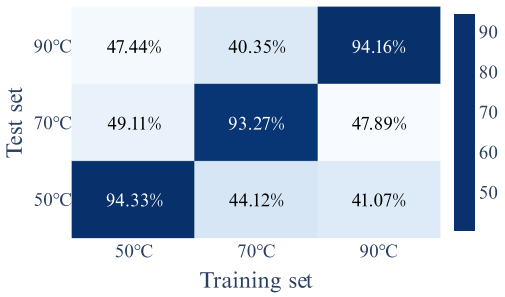

Fig. 22. *LiqRay* + is able to accurately identify liquids when the data in the test set and that in the training set are collected at the same temperature.

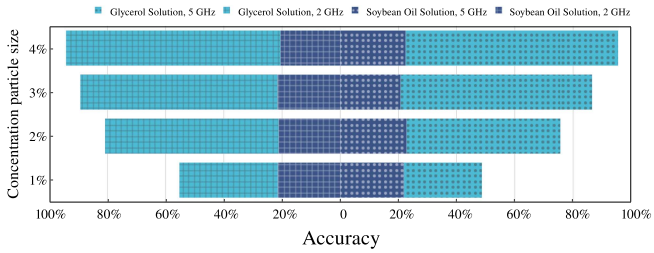

Fig. 23. Identification performance of solutions with different oil-based liquids.

at three temperatures, which are 50°C, 70°C, and 90°C. In order to ensure a constant temperature during the data collection process, we use a kettle with temperature control function as the container, whose volume is about 2L, and the kettle's material is glass. For each case, we collect 50 times independently. Then a KNN (k=1) classifier is used to identify the concentration of the liquid.

The results are shown in Fig. 22. When the data in the training set and the data in the test set are collected at the same temperature, *LiqRay*$^+$ can accurately identify the liquid. At three different temperatures, the accuracy rate exceeded 93%. But when the data of the test set and the data of the training set are collected at different temperatures, *LiqRay*$^+$ has a poor ability to identify liquids. We believe the reason is that the complex permittivity of the same liquid changes with temperature. Therefore, liquid features collected at one temperature cannot ef- fectively distinguish data collected at another temperature.

C. Macro Benchmark

LiqRay$^+$*'s Performance in Different Environments With Different Vessels.* As shown in Fig. 12, we test *LiqRay*$^+$'s ability to identify liquids in a hall environment, a simulated living room environment, and a laboratory environment. For each environment, we pour the test liquids into five different shape glass vessels, including cube, cylinder, and three irregular shapes. The liquids are with different concentrations from 0% to 10% at a step size of 1%, 45%, 46% and 78% with water. As shown in Fig. 21, vessels of different shapes have similar accuracy rates. The difference in accuracy between different vessels is less than 4%. and the difference in accuracy between different environments is less than 3%.

NaCl and Sucrose Concentration Detection: Regarding people with high blood pressure and diabetes, controlling salt and sugar intake can help keep them healthy. We perform concentration identification for sodium chloride solutions and sucrose solutions. We dissolve *NaCl* and sucrose in water with a particle size of 2%, and use the KNN method to identify them. The results are shown in Fig. 20, and the identification accuracy is over 93%.

Oil-Based Concentration Detection: We test *LiqRay*$^+$'s ability to identify oil-based liquids using mineral oil as the solvent and soybean oil and glycerol as the solute, respectively. A resin vessel of size 30 cm × 30 cm × 8 cm is used to hold the liquid. We use mineral oil as the solvent and soybean oil and glycerol are used as the solute, respectively. The concentration of the solution is varied from 1% to 20%. For each concentration, data are collected 50 times independently. Then a KNN (k=1) classifier is used to identify the concentration of the liquid. As shown in Fig. 23. *LiqRay*$^+$ can distinguish 2% particle size glycerol solutions with over 78% accuracy. But for the soybean oil solution, *LiqRay*$^+$ has difficulty distinguishing effectively. We believe the reason is that the attenuation of electromagnetic waves is more pronounced in glycerol than in soybean oil [48], [49], [50]. Since the liquid features depend on the attenuation factor of the liquid, it is difficult to effectively distinguish between lossless media.

VI. Practical Issues

In this section, we provide some theoretical analysis of the usability of the system. Three main practical issues are discussed:

- Is the system receiving interference from diffraction? Electromagnetic waves diffract when the size of the medium is similar to the wavelength. This makes it difficult for us to approximate wave propagation with rays. And *LiqRay*$^+$ is built based on the alleged tracking model. Therefore, we discuss the effect of diffraction. Theoretical analysis shows that, for our chosen container and frequency, the diffraction phenomenon is insignificant.
- Is the USRP device good enough to distinguish the two signals? The USRP device has a higher noise floor and the *LiqRay*$^+$ has a smaller distance between the two receiving antennas. We investigated whether the difference between the two signals is large enough that it is not drowned out by USRP noise.
- Are the two receiving antennas coherent? When two antennas are in close proximity, they interfere with each other. We design experiments to explore whether the two receiving antennas of *LiqRay*$^+$ are coherent. Experiments show that, according to our system design, the coherence of the two receiving antennas is small.

A. The Impact of Diffraction

LiqRay + is built on the ray tracing model [21]. When the size of the obstacle is similar to the wavelength, the diffraction phenomenon can make the ray tracing model unsuitable [41].

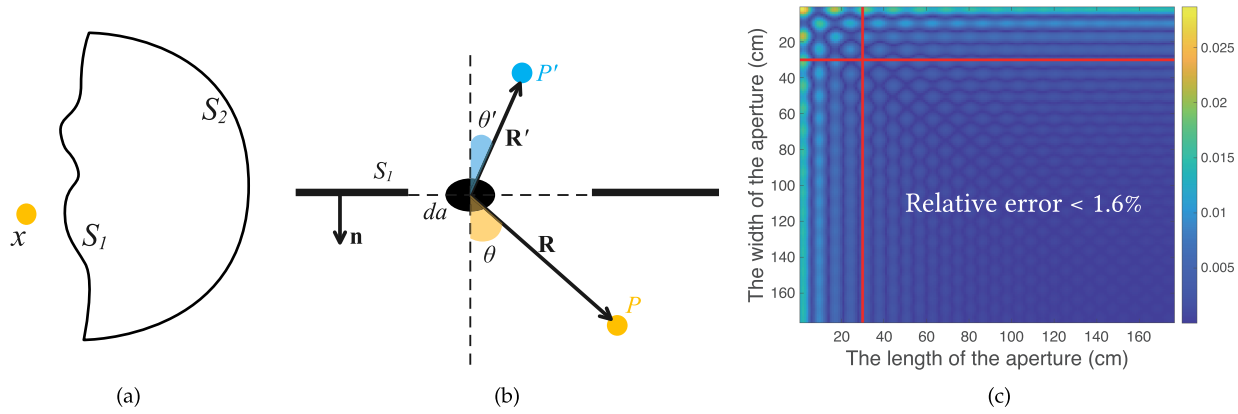

Fig. 24. Schematic diagram and calculation result of Kirchhoff integral. (a) The wave perturbation at the point x outside the closed surface $S1 + S2$ can be expressed as a function of all wave perturbations located on the closed surface and its gradient. (b) Diffraction geometry for a plane screen with apertures, a point source at P', and an observation point at P. (c) The relative difference between the results of the Kirchhoff integration and the ray tracing model is small.

Therefore, we analyze the effect of diffraction by theoretical calculations.

When the Vessel Size is Large, the Effect of Diffraction Can be Ignored: When the length and width of the vessel exceed 30 cm, the relative error on the results between the Kirchhoff integration [19] and the ray tracing model is less than 1.6%. We believe that the model described in the paper is applicable in this case. Diffraction phenomena can be explained using Huygens' principle [51], and Kirchhoff's integral can be approximated using Huygens' principle [41]. According to Kirchhoff's integral theorem, the field strength of a point P in a closed surface can be regarded as the sum of the effects of each point on the surface on P. As shown in Fig. 24(b), the electromagnetic waves emitted by the point source P' reaches the point P in space through the small hole on the screen. With Kirchhoff approximation [52], (20) can be written as:

$$E(P) = \frac{ik}{2\pi} \oint_{aperture} \frac{e^{ikR}}{R} \frac{e^{ikR'}}{R'} cos\theta \left(1 + \frac{i}{kR}\right) da, \quad (20)$$

where R and R' are the distances from the element of area da in the aperture to the points P and P', respectively. The angle θ and θ' are those between $\mathbf{R}$ and $\mathbf{n}$, and $\mathbf{R}'$ and $\mathbf{n}'$, respectively. We perform simulation calculations based on (20) and our experimental setup. Specifically, the distance from the light source P' to the screen of the screen is 0.5m, and the distance from the observation point to the screen is 1.5 cm. Fig. 24(c) shows the difference between the integration results and the ray tracing model. When the vessel size is larger than 30 cm, the relative difference is less than 1.6%, so we believe that our model can be applied in this case.

For smaller size vessels, we rigorously calculate the distribution of the electromagnetic field around the vessel using the Mie scattering model. *The analysis results show that with the features designed in the paper, even if the vessel material changes, we can use the KNN model to distinguish different liquids.*

For obstacles whose size parameters are similar to the wavelength of electromagnetic waves, Mie scattering theory can be used to analyze the scattered light field [53]. As shown in Fig. 25(a), the axis of a concentric infinite cylindrical obstacle is parallel to the z-axis. The total cylinder is r_1 and the radius of the inner cylinder is given by r_2. The incident wave propagates along the positive x direction, and the electric field direction is along the positive z direction. The scattered field outside the cylinder in the xOy plane can be expressed as [54]

$$E(r,\theta) = -E_0 \sum_{n=-\infty}^{\infty} (j)^{-n} b_n H_n(m_0 kr) e^{in\theta + i\omega t} \quad (21)$$

where the coordinates r and θ are defined by $x = rcos\theta$, $y = rsin\theta$. The Hankel function of the second kind, $H_n(Z)$, is defined by $H_n(Z) = J_n(Z) - iN_n(Z)$, where J_n and N_n are the spherical Bessel functions of the first and second kind, respectively. The wave number, k, is defined by $k = \frac{2\pi}{\lambda}$, where λ is the wavelength of the electromagnetic waves in the dielectric outside the obstacle. The coefficient b_n is same to the definition of [54], where m_0, m_1, and m_2 are the refractive indices of the dielectric outside the cylinder, the outer cylindrical dielectric, and the inner cylindrical dielectric, respectively. The first derivatives of J_n and H_n are denoted by J'_n and H'_n, respectively.

We use the Lichtenecker formula [55], [56] to obtain approximate values for different concentrations of alcohol solutions. Specifically, the permittivity of the mixed liquid, ϵ, can be expressed as

$$ln(\epsilon) = Cln(\epsilon_{alc}) + (1 - C)ln(\epsilon_{water}) \quad (22)$$

where C is the volume fraction ratio of alcohol, ϵ_{alc} is the permittivity of anhydrous ethanol, and ϵ_{water} is the permittivity of water. We set the inner dielectric of the cylinder to an alcohol solution, and the outer dielectric to different materials [57], [58], including wood, glass, hard paper, ceramic, and PVC. We set the width of the vessel to 5 cm, the thickness of the vessel to 3 mm, and the angle between the two receiving antennas to be $\pi/6$. We calculate data at frequencies of 1.7 GHz, 2 GHz, 2.4 GHz, and 2.6 GHz. Fig. 25(b) shows their intra- and inter-class distance. We find that the difference caused by different materials is smaller than that caused by different concentrations, which indicates that the distinction can be done using the KNN classifier.

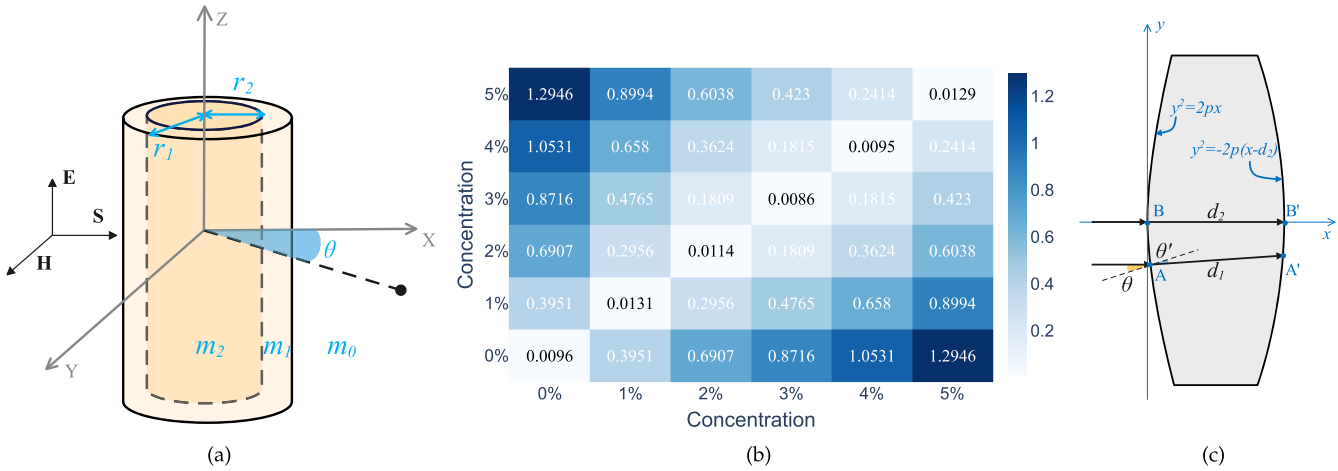

Fig. 25. Using Mie scattering theory to verify the feasibility of KNN classification. (a) The electromagnetic wave propagating along the positive x-axis is vertically incident on a double-layer cylinder. (b) When the vessel materials are different, the intra-class distance of the concentration is smaller than the inter-class distance. (c) The deformed vessel.

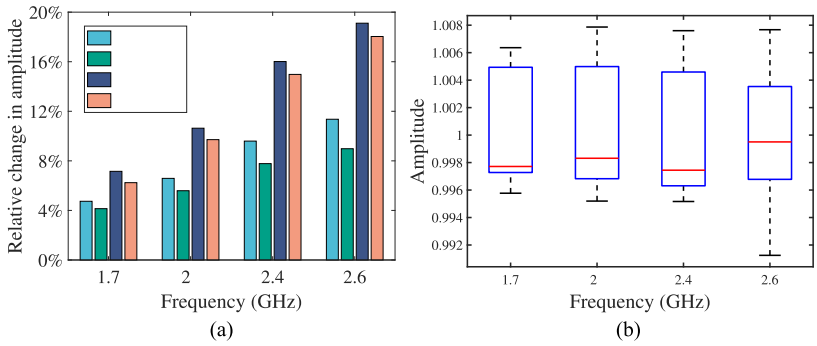

Fig. 26. USRP devices can distinguish between two RF signals. (a) The difference between the two receiving antennas is usually more than 8%. (b) The standard deviation of repeated collection data is less than 0.005.

B. Ability of USRP to Distinguish Signals

Theoretically, as long as there is a difference in the distance that the signal travels in the liquid, the amplitude of the signal received by the two receiving antennas will be different. However, due to the noise of the receiving device, when the transmission distance is small enough, the receiving device cannot distinguish the two signals. We analyze the difference between the signal amplitudes of the two receiving antennas of *LiqRay*$^+$. We explore the limits of USRP's ability to discriminate between signals.

Our Evaluations Show That the Difference Between the Two Signals is Typically Greater Than 8%: Due to the slight deformation of the vessel and the rapid attenuation of the signal in the liquid, the amplitude difference between the two receiving antennas is usually more than 8%, which is shown in Fig. 26(a).

In Addition, We Explore the Limits of USRP to Distinguish Signals: For four different frequencies (1.7 GHz, 2 GHz, 2.4 GHz and 2.6 GHz), we independently acquire data 200 times in an empty hall. For each acquired data, we use a Gaussian filter to remove noise. In order to make the signals of different frequencies have the same dimension (the gain of the antenna to the signals of different frequencies is different), we linearly scale the amplitudes of the signals of different frequencies so that their mean is 1. The results are shown in Fig. 26(b). The standard deviation of data collected at different times of the same frequency does not exceed 0.005. Therefore, we believe that the difference between the signals that can be distinguished by USRP device should be no less than 1%. For a 2 GHz signal, the transmission distance of the signal in water is greater than 1.6 mm, and when the frequency rises to 5 GHz, this threshold is reduced to 0.6 mm.

Due to the Thin Walls of the Vessel, the Vessel Will Deform Slightly After Being Filled With Liquid: At this time, Δd is greater than 6 mm. Fig. 13(a) shows the vessel used for the experiment. Due to the thin walls of the vessel, when the vessel is filled with water, it deforms to about 13 cm wide in the middle and about 8 cm wide on the sides. We model the vessel, which is shown in Fig. 25(c). For the convenience of calculation, we approximate the two sides of the deformation as parabolas, and their equations are $y^2 = 2px$ and $y^2 = -2p(x - d_2)$, respectively. The two RF signals are incident from points $A(x_a, y_a)$

and $B(x_b, y_b)$, respectively, and the transmission distances in the liquid are d_1 and d_2, respectively. The exit points of the two signals are $A'(x'_a, y'_a)$ and $B'(x'_b, y'_b)$. They should satisfy the equation:

$$\begin{cases} y_a^2 = 2px_a,\ y'^2_a = -2p(x'_a - d_2) \\ y_b^2 = 2px_b,\ y'^2_b = -2p(x'_b - d_2) \\ \frac{sin\theta}{sin\theta'} = \frac{n_{liq}}{n_{air}} \end{cases} \tag{23}$$

where n_{liq} is the refractive index of the liquid, n_{air} is the refractive index of the air, p is the propagation constant, and θ and θ' are the angles of the incident and transmitted signals. For the situation in Fig. 25(c), we let $p = 45$ and $d_2 = 13$ cm. When $x = 5$ cm, the difference $d_2 - d_1$ of the signal transmission distance in the liquid is about 6 mm.

C. Antenna Coupling

In deployment, the distance between two receiving antennas may be less than half a wavelength. Antenna coupling affects the amplitude of the received signal because the mutual impedance among multiple antennas affects the equivalent impedance of the receiving antenna [59]. In this case, the mutual coupling of the antennas may affect the strength of the received signal. Compared with the case where the antenna distance is 10 cm, the variation of the reflection coefficient when the antenna distance is 4 cm is less than 0.4 dB, which means that the difference in amplitude is less than 2%. Therefore, we believe that the mutual coupling of the antennas does not affect the amplitude, following the experimental setup in the paper.

Part of the electromagnetic waves radiated to the antenna will be received by the antenna, and the other part will be reflected. The ratio of these two parts is called reflection coefficient, which is defined as [60]

$$\rho = \sqrt{\frac{P_{ref}}{P_{inc}}}, \tag{24}$$

where P_{ref} is the power of the reflected signal, and P_{inc} is the power of the incident signal. The reflection coefficient depends on how well the antenna impedances are matched [59]. Antenna coupling affects the amplitude of the received signal because the mutual impedance between multiple antennas changes the equivalent impedance of the receiving antenna [59]. We use the ENA vector network analyzer (KEYSIGHT E5071 C) to test the change of the reflection coefficient of the antenna when the distance between the two receiving antennas is different, and the results are shown in the Fig. 27. Compared with 10 cm, when the antenna spacing is 4 cm, the change of the reflection coefficient does not exceed 0.4 dB, which indicates that the change of the received signal amplitude does not exceed 2%. The diameter of the antenna used for liquid identification is 3 cm and the distance between the antennas is more than 4 cm, so we believe that the antenna coupling does not affect the amplitude of the received signal.

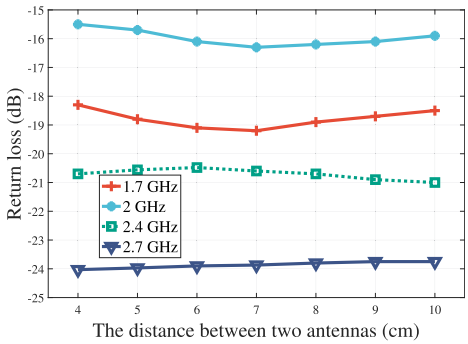

Fig. 27. Reflection coefficient are relatively stable across different distances.

D. Other Limitations and Future Work

We construct features based on the attenuation factor of the liquid for liquid identification. This results in *LiqRay*$^+$ being unable to distinguish between different kinds of lossless media. But we notice that although wireless signals decay very slowly in lossless media, the signals travel at different speeds in different media. In future work, we plan to combine the phase of the signal to complete the identification of lossless media.

The Tradeoff Between Incident Angle Robustness and Higher Accuracy: Compared to the original conference version [38], the average solution concentration classification drops by about 2%. We believe this is due to the extra division we performed in Liqray+ (Section IV-B). This can add nonlinearity errors, especially if the dividend is small. We discuss the tradeoffs between the two in this subsection.

The refraction ratio of the signal depends on the type of medium and the angle of incidence. The refractive ratio of different liquids is different in sensitivity to changes in the angle of incidence. we calculate the relationship between the refractive ratio and the incident angle. The results show that the refractive ratio of some liquids (such as oil) hardly changes with the incident angle when the incident angle is less than 1 rad. But for another part of the liquid, such as water, their refraction ratio is more sensitive to changes in the angle of incidence. Therefore, when the incident angle is unknown, we recommend using the method proposed by *LiqRay*$^+$ to construct liquid features, and when the incident angle is not large, such as less than 0.4 radians, we can use the method proposed by LiqRay [38] to construct liquid features

The Limitation of Liquid Height: When the liquid is high enough, the identification effect of the liquid is better, because at this time most of the RF signal reaches the receiving antenna through the liquid. And when the liquid is relatively low, the liquid identification is still disturbed despite using our height model. We believe that the main reason is that when the liquid height is small, the electromagnetic wave passing through the liquid no longer satisfies the plane wave assumption. For a fine-grained antenna, when the pitch angle is large enough, the signal becomes weaker, and the wave no longer propagates along the radial direction. *LiqRay*$^+$ is based on the assumption that the incident wave is a plane wave. Therefore, the method proposed

by *LiqRay*$^+$ may no longer be applicable when the liquid level is low. If we can build a more accurate perception model based on the radiation characteristics of the antenna, it will help to further remove the limitation of liquid height. In future work, we will actively explore more general perception schemes.

VII. Related Work

RF-based Liquid Detection Method: Recently, in the field of liquid identification, researchers have proposed many excellent systems based on RF [5], [6], [7], [8]. Those methods can be divided into two categories, one is data-driven, which requires pre-trained features to distinguish different liquids; the other is model-driven, which builds models to obtain the physical or chemical parameters of the liquid itself (such as complex permittivity).

(1) *Data-driven method:* Tagscan [8] extracts the RSSI and phase change as features from RFID tag reading to create a database and classify 10 liquids. Tagtag [10] propose to attach one RFID tag on the target of interest for liquid testing, which can detect fake alcohol, baby formula adulteration, fake luxury CHANEL perfume, and expired milk by comparing with the training set. FG-LiquID [12] designs a novel neural network for sensing liquids using millimeter wave radar, which can identify 30 different liquids in a fine-grained manner. In addition to not being able to identify the unknown liquids, it is inconvenient to build a database containing lots of kinds of solutions. Therefore, we use a model-driven approach to construct the system with the attenuation factor.

(2) *Model-driven method:* LiquID [5] uses the amplitude and phase of the signal to solve the equation to obtain the complex permittivity of the liquid, which is able to identify 33 kinds of liquids. Using mechanical waves, Vi-Liquid [13] builds a model to compute the viscosity of the liquid, which realizes the identification of 30 kinds of liquids. But these methods usually rely on prior knowledge, such as the material and width of the vessel. Having built a dual-antenna model and extracted the relative frequency response factor as a feature of the liquid, we construct a vessel-independent system.

They only identify liquids in the 2D ranges without considering the relative height of the solution to the antenna. We construct the distribution model of the electric field and eliminate the influence of height by using the change of the electric field when the transmitting antenna is displaced and completed the solution identification in the 3D range.

In summary, *LiqRay*$^+$ differs from previous outstanding work in three main ways. (1) Container material independence. There are many excellent previous works on non-contact liquid identifi- cation. Due to the variety of materials used to hold liquid containers in daily life, sensing independent of container materials will provide more potential applications for ubiquitous perception. (2) Container width independence. Many previous outstanding works take the width information of containers as prior knowledge. But in the process of actual deployment, it is not easy to measure the size of the container in advance. Therefore, we designed a dual-antenna model so that *LiqRay*$^+$ can identify liquids without being affected by the width of the container. (3) Liquid height independent. Due to the different transmission characteristics of RF signals in air and in liquids, excellent work previously required multiple antennas at the height of the liquid to be measured. However, a large number of sub-6 GHz antennas (such as router antennas) are longer than 15 cm, and the size of many liquids to be measured is less than 10 cm. Based on the radiation characteristics of the antenna, *LiqRay*$^+$ proposes an electromagnetic difference model, which allows us to identify liquids that are independent of the liquid height.

Traditional Liquid Identification Methods: Traditionally, material identification requires the use of expensive specialized equipment to provide data [61], [62], [63], [64]. In addition to expensive equipment, these methods typically require immersing the probe in a solution to collect the signal and further analyze the spectral information with a spectrometer.

Optical and Camera Based Liquid Detection Method: Recent research on optical and camera-based liquid detection method has many different problem-solving theories and meaningful applications [6], [7], [65], [66]. Smart-U [6] can identify food or liquid in the spoon by employing the LEDs and photodiodes. However, these methods are not easy to deploy in daily life. CapCam [66] uses the phone's camera to capture the ripples created by vibrations in the solution to identify the solution. But it only identifies clear solutions.

VIII. Conclusion

This paper presents *LiqRay*$^+$, a contactless and fine-grained system that can use RF signals to identify unknown liquids. We develop a new computational model independent of the vessel material and width, as well as the liquid height, which allows us to identify unknown liquids in unknown vessels. Our comprehensive experiments show that *LiqRay*$^+$ can discriminate between alcoholic liquids with a concentration difference of 1%, monitoring sugar and salt intake. It can cope with different vessels and liquid heights. Our model-driven scheme is making efforts to cultivate liquid identification system pervasive and robust enough for more applications and scenarios.

References

[1] C. Blom and J. Mellema, "Torsion pendula with electromagnetic drive and detection system for measuring the complex shear modulus of liquids in the frequency range 80–2500 Hz," *Rheologica Acta*, vol. 23, no. 1, pp. 98–105, 1984.
[2] J. de Vicente, M. T. López-López, J. D. Durán, and F. González-Caballero, "Shear flow behavior of confined magnetorheological fluids at low magnetic field strengths," *Rheologica Acta*, vol. 44, no. 1, pp. 94–103, 2004.
[3] A. A. Note, "Agilent basics of measuring the dielectric properties of materials," *Agilent Literature Number*, pp. 1–34, 2006.
[4] C. Riesch, E. K. Reichel, F. Keplinger, and B. Jakoby, "Characterizing vibrating cantilevers for liquid viscosity and density sensing," *J. Sensors*, vol. 2008, p. 9, 2008, Art. no. 697062.
[5] A. Dhekne, M. Gowda, Y. Zhao, H. Hassanieh, and R. R. Choudhury, "Liquid: A wireless liquid identifier," in *Proc. 16th Annu. Int. Conf. Mobile Syst. Appl. Serv.*, 2018, pp. 442–454.
[6] Q. Huang, Z. Yang, and Q. Zhang, "Smart-U: Smart utensils know what you eat," in *Proc. IEEE Conf. Comput. Commun.*, 2018, pp. 1439–1447.
[7] T. Rahman, A. T. Adams, P. Schein, A. Jain, D. Erickson, and T. Choudhury, "Nutrilyzer: A mobile system for characterizing liquid food with photoacoustic effect," in *Proc. 14th ACM Conf. Embedded Netw. Sensor Syst.*, 2016, pp. 123–136.

[8] J. Wang, J. Xiong, X. Chen, H. Jiang, R. K. Balan, and D. Fang, "TagScan: Simultaneous target imaging and material identification with commodity RFID devices," in *Proc. 23rd Annu. Int. Conf. Mobile Comput. Netw.*, 2017, pp. 288–300.

[9] P. Donato, F. Cacciola, P. Q. Tranchida, P. Dugo, and L. Mondello, "Mass spectrometry detection in comprehensive liquid chromatography: Basic concepts, instrumental aspects, applications and trends," *Mass Spectrometry Rev.*, vol. 31, no. 5, pp. 523–559, 2012.

[10] B. Xie et al., "Tagtag: Material sensing with commodity RFID," in *Proc. 17th Conf. Embedded Networked Sensor Syst.*, New York, NY, USA, 2019, pp. 338–350.

[11] C. Feng et al., "WiMi: Target material identification with commodity Wi-Fi devices," in *Proc. IEEE 39th Int. Conf. Distrib. Comput. Syst.*, 2019, pp. 700–710.

[12] Y. Liang, A. Zhou, H. Zhang, X. Wen, and H. Ma, "FG-LiquID: A contactless fine-grained liquid identifier by pushing the limits of millimeter-wave sensing," in *Proc. ACM Interact. Mob. Wearable Ubiquitous Technol.*, vol. 5, pp. 1–27, Sep. 2021.

[13] Y. Huang, K. Chen, Y. Huang, L. Wang, and K. Wu, "Vi-liquid: Unknown liquid identification with your smartphone vibration," in *Proc. 27th Annu. Int. Conf. Mobile Comput. Netw.*, 2021, pp. 174–187.

[14] J. D. Kraus and R. J. Marhefka, *Antenna: For All Applications (Third Editions)[m]*, Beijing, China: Publishing House of Electronics Industry, 2011.

[15] M. A. Uman, D. K. McLain, and E. P. Krider, "The electromagnetic radiation from a finite antenna," *Amer. J. Phys.*, vol. 43, no. 1, pp. 33–38, 1975.

[16] A. Salinas, R. G. Martin, A. R. Bretones, and I. S. Garcia, "Modelling of straight thin wires using time-domain electric field integral equations," *IEE Proce.-Microw. Antennas Propag.*, vol. 141, no. 2, pp. 123–126, 1994.

[17] Amazon, "COCA COLA CANS 330ML PK24 A00768 VRBCOKE," [EB/OL], 2022. [Online]. Available: https://www.amazon.com/COCA-COLA-330ML-A00768-VRBCOKE/dp/B0051GNHJ4

[18] R. P. Feynman, R. B. Leighton, and M. Sands, "The Feynman lectures on physics," in *The New Millennium Edition: Mainly Mechanics, Radiation, and Heat*, New York, NY, USA: Basic books, 2011.

[19] J. D. Jackson and R. F. Fox, "Classical electrodynamics, 3rd ed.," *Amer. J. Phys.*, vol. 67, no. 9, pp. 841–842, Sep. 1999. [Online]. Available: https://pubs.aip.org/aapt/ajp/article-pdf/67/9/841/7528211/841_2_online.pdf

[20] F. Stern and C. Weaver, "Dispersion of dielectric permittivity due to space-charge polarization," *J. Phys. C: Solid State Phys.*, vol. 3, no. 8, 1970, Art. no. 1736.

[21] D. Tse and P. Viswanath, *Fundamentals of Wireless Communication*. Cambridge, U.K.: Cambridge Univ. Press, 2005.

[22] A. Iyer, C. Rosenberg, and A. Karnik, "What is the right model for wireless channel interference?," *IEEE Trans. Wireless Commun.*, vol. 8, no. 5, pp. 2662–2671, May 2009.

[23] X. Bohigas and J. Tejada, "Dielectric characterization of alcoholic beverages and solutions of ethanol in water under microwave radiation in the 1–20 Ghz range," *Food Res. Int.*, vol. 43, no. 6, pp. 1607–1613, 2010.

[24] J. Krupka, "Frequency domain complex permittivity measurements at microwave frequencies," *Meas. Sci. Technol.*, vol. 17, no. 6, 2006, Art. no. R55.

[25] R. Böhmer, M. Maglione, P. Lunkenheimer, and A. Loidl, "Radio-frequency dielectric measurements at temperatures from 10 to 450 k," *J. Appl. Phys.*, vol. 65, no. 3, pp. 901–904, 1989.

[26] A. P. Gregory and R. N. Clarke, "Tables of the complex permittivity of dielectric reference liquids at frequencies up to 5 GHz," Tech. Rep., 2012. [Online]. Available: http://eprintspublications.npl.co.uk/4347/

[27] J. G. Kirkwood, "On the theory of dielectric polarization," *J. Chem. Phys.*, vol. 4, no. 9, pp. 592–601, 1936.

[28] J. G. Kirkwood, "The dielectric polarization of polar liquids," *J. Chem. Phys.*, vol. 7, no. 10, pp. 911–919, 1939.

[29] S. Jiang and S. Georgakopoulos, "Electromagnetic wave propagation into fresh water," *J. Electromagn. Anal. Appl.*, vol. 3, pp. 261–266, 2011.

[30] I. S. Nefedov, A. J. Viitanen, and S. A. Tretyakov, "Electromagnetic wave refraction at an interface of a double wire medium," *Phys. Rev. B*, vol. 72, no. 24, 2005, Art. no. 245113.

[31] C. H. Papas, *Theory of Electromagnetic Wave Propagation*. Chelmsford, MA, USA: Courier Corporation, 2014.

[32] D. Fleisch, *A student's Guide to Maxwell's Equations*. Cambridge, U.K.: Cambridge Univ. Press, 2008.

[33] H. A. Von and R. Arthur, *Dielectrics and Waves* Cambridge, MA, USA: MIT Press, 1954.

[34] P. Bobrov, A. Lapina, and A. Repin, "Effect of the rock/water/air interaction on the complex dielectric permittivity and electromagnetic waves attenuation in water-saturated sandstones," in *Proc. Prog. Electromagnetics Res. Symp.*, 2015, pp. 1877–1879.

[35] A. Ishimaru, *Electromagnetic Wave Propagation, Radiation, and Scattering: From Fundamentals to Applications*. Hoboken, NJ, USA: Wiley, 2017.

[36] Y. Lee et al., *Antenna Circuit Design for RFID Applications*, Chandler, Az, USA: Microchip Technology Inc., 2003.

[37] D. Poljak, S. Antonijevic, K. E. K. Drissi, and K. Kerroum, "Transient response of straight thin wires located at different heights above a ground plane using antenna theory and transmission line approach," *IEEE Trans. Electromagn. Compat.*, vol. 52, no. 1, pp. 108–116, Feb. 2010.

[38] F. Shang, P. Yang, Y. Yan, and X.-Y. Li, "LiqRay: Non-invasive and fine-grained liquid recognition system," in *Proc. 28th Annu. Int. Conf. Mobile Comput. Netw.*, 2022, pp. 296–309.

[39] A. Shaw, A. Al-Shamma'a, S. Wylie, and D. Toal, "Experimental investigations of electromagnetic wave propagation in seawater," in *Proc. Eur. Microw. Conf.*, 2006, pp. 572–575.

[40] D. J. Griffiths and C. Inglefield, "Introduction to electrodynamics," *Amer. J. Phys.*, vol. 73, no. 6, p.574, Jun. 2005. [Online]. Available: https://doi.org/10.1119/1.4766311

[41] M. Born and E. Wolf, *Principles of Optics: Electromagnetic Theory of Propagation, Interference and Diffraction of Light*. Amsterdam, The Netherlands: Elsevier, 2013.

[42] U. Kaatze, "Complex permittivity of water as a function of frequency and temperature," *J. Chem. Eng. Data*, vol. 34, no. 4, pp. 371–374, 1989.

[43] B. Quan et al., "Dielectric polarization in electromagnetic wave absorption: Review and perspective," *J. Alloys Compounds*, vol. 728, pp. 1065–1075, 2017.

[44] H. J. Liebe, G. A. Hufford, and T. Manabe, "A model for the complex permittivity of water at frequencies below 1 THz," *Int. J. Infrared Millimeter Waves*, vol. 12, no. 7, pp. 659–675, 1991.

[45] V. Doric, D. Poljak, J. Paul, and C. Christopoulos, "Modeling of a straight thin wire: Comparison of antenna approach and transmission line model," in *Proc. 15th Int. Conf. Softw. Telecommun. Comput. Netw.*, 2007, pp. 1–3.

[46] J. Terry and J. Heiskala, *OFDM Wireless LANs: A Theoretical and Practical Guide*. Carmel, IN, USA: Sams Publishing, 2002.

[47] L. Rokach and O. Maimon, "Clustering methods," in *Data Mining and Knowledge Discovery Handbook*, Berlin, Germany: Springer, 2005, pp. 321–352.

[48] J. Corach, E. F. Galván, P. A. Sorichetti, and S. D. Romano, "Estimation of the composition of soybean biodiesel/soybean oil blends from permittivity measurements," *Fuel*, vol. 235, pp. 1309–1315, 2019.

[49] M. Brady and S. Stuchly, "Dielectric dispersion of glycerol from 2.0 to 4.0 GHz," *J. Chem. Phys.*, vol. 74, no. 6, pp. 3632–3633, 1981.

[50] R. Behrends, K. Fuchs, U. Kaatze, Y. Hayashi, and Y. Feldman, "Dielectric properties of glycerol/water mixtures at temperatures between 10 and 50," *J. Chem. Phys.*, vol. 124, no. 14, 2006, Art. no. 144512.

[51] C. Huygens, *Traité De La Lumière*. Paris, France: Gauthier-Villars, 1920.

[52] E. I. Thorsos, "The validity of the kirchhoff approximation for rough surface scattering using a Gaussian roughness spectrum," *J. Acoustical Soc. Amer.*, vol. 83, no. 1, pp. 78–92, 1988.

[53] H. C. Hulst and H. C. van de Hulst, *Light Scattering by Small Particles*, Chelmsford, MA, USA: Courier Corporation, 1981.

[54] M. Kerker and E. Matijević, "Scattering of electromagnetic waves from concentric infinite cylinders," *JOSA*, vol. 51, no. 5, pp. 506–508, 1961.

[55] R. Simpkin, "Derivation of lichtenecker's logarithmic mixture formula from Maxwell's equations," *IEEE Trans. Microw. Theory Techn.*, vol. 58, no. 3, pp. 545–550, Mar. 2010.

[56] K. Lichtenecker, "Die dielektrizitätskonstante natürlicher und künstlicher mischkörper," *Physikalische Zeitschrift*, vol. 27, pp. 115–158, 1926.

[57] A. Ćenanović, S. Martius, A. Kilian, J. Schür, and L.-P. Schmidt, "Non destructive complex permittivity determination of glass material with planar and convex surface," in *Proc. German Microw. Conf.*, 2011, pp. 1–4.

[58] M. Bendaoued, J. Terhzaz, and R. Mandry, "Determining the complex permittivity of building dielectric materials using a propagation constant measurement," *Int. J. Elect. Comput. Eng.*, vol. 7, no. 4, 2017, Art. no. 1681.

[59] J. D. Kraus and R. J. Marhefka, *Antennas for All Applications. Antennas for All Applications*, New York, NY, USA: McGraw Hill, 2003.

[60] T. S. Bird, "Definition and misuse of return loss [report of the transactions editor-in-chief]," *IEEE Antennas Propag. Mag.*, vol. 51, no. 2, pp. 166–167, Apr. 2009.
[61] M. Szymańska-Chargot, J. Cybulska, and A. Zdunek, "Sensing the structural differences in cellulose from apple and bacterial cell wall materials by raman and FT-IR spectroscopy," *Sensors*, vol. 11, no. 6, pp. 5543–5560, 2011.
[62] G. Tsiminis, F. Chu, S. C. Warren-Smith, N. A. Spooner, and T. M. Monro, "Identification and quantification of explosives in nanolitre solution volumes by Raman spectroscopy in suspended core optical fibers," *Sensors*, vol. 13, no. 10, pp. 13163–13177, 2013.
[63] J. F. Federici, "Review of moisture and liquid detection and mapping using terahertz imaging," *J. Infrared Millimeter Terahertz Waves*, vol. 33, no. 2, pp. 97–126, 2012.
[64] C. Blakley, J. Carmody, and M. Vestal, "Liquid chromatograph-mass spectrometer for analysis of nonvolatile samples," *Anal. Chem.*, vol. 52, no. 11, pp. 1636–1641, 1980.
[65] H. Matsui, T. Hashizume, and K. Yatani, "Al-light: An alcohol-sensing smart ice cube," in *Proc. ACM Interactive Mobile Wearable Ubiquitous Technol.*, vol. 2, no. 3, pp. 1–20, 2018.
[66] S. Yue and D. Katabi, "Liquid testing with your smartphone," in *Proc. 17th Annu. Int. Conf. Mobile Syst. Appl. Serv.*, 2019, pp. 275–286.

Fei Shang received the BS degree in electronic information engineering from the College of Information Science and Technology, Northwest University, China, in 2020. He is currently working toward the PhD degree with the University of Science and Technology of China. His current research interests include wireless sensing systems, wireless networks, and IoT Technology.

Panlong Yang (Member, IEEE) received the BS, MS, and PhD degrees in communication and information system from the Nanjing Institute of Communication Engineering, China, in 1999, 2002, and 2005 respectively. He is now a professor with the College of Computer Science and Technology, University of Science and Technology of China. His research interests include wireless mesh networks, wireless sensor networks, and cognitive radio networks. He is a member of the IEEE Computer Society and ACM SIGMOBILE Society.

Yubo Yan (Member, IEEE) received the BS, MS, and PhD degrees in communication and information system from the PLA University of Science and Technology, China, in 2006, 2011 and 2017 respectively. He is now an associate professor with the University of Science and Technology of China. His current research interests include Internet of Things, wireless networks, intelligent sensing, and mobile computing. He is a member of the IEEE Communications Society.

Xiang-Yang Li (Fellow, IEEE) received the bachelor's degree from the Department of Computer Science, Tsinghua University, China, in 1995, and the MS and PhD degrees from the Department of Computer Science, University of Illinois at Urbana-Champaign, in 2000 and 2001. He is a professor and executive dean with the School of Computer Science and Technology, USTC. He is an ACM fellow (2019) and ACM distinguished scientist (2014). He was a full professor with the Computer Science Department, IIT. His research interests include artificial intelligence of Things (AIOT), privacy and security of AIOT, and data sharing and trading. He and his students won several best paper awards, including MobiCom.